ELSEVIER

Journal of Neuroscience Methods 156 (2006) 333–341

JOURNAL OF NEUROSCIENCE METHODS

www.elsevier.com/locate/jneumeth

# Practical nerve morphometry

Fulvio Urso-Baiarda *, Adriaan O. Grobbelaar

*Restoration of Appearance and Function Trust (RAFT), Leopold Muller Building, Mount Vernon Hospital, Rickmansworth Road, Northwood, Middlesex HA6 2RN, United Kingdom*

Received 12 January 2006; received in revised form 6 February 2006; accepted 13 February 2006

**Abstract**

Histopathological examination of peripheral nerves is often complemented by morphometric analysis in both clinical and research settings. However, existing manual or semi-automated methods are highly tedious, labour intensive and time-consuming, whereas fully automated morphometry is prone to error from the conversion of maldetected particles to spurious data. Both fully and interactive-automated morphometry have significant hardware requirements and may be difficult to implement. A new method for nerve morphometry is described aiming to combine the speed of automated morphometry with the accuracy of manual or semi-automated methods, and requiring only a digital image of the nerve section and two widely available software packages. Comparison with a standard digitizer pen method of nerve morphometry without sampling yielded statistically similar axon counts, mean area assessments and axonal area frequency distribution histograms, with assessment times of the new method between 35% and 45% of those of the standard method. This has widespread potential experimental and clinical applications and offers a means of relieving much of the tedium currently associated with nerve morphometry.


*Keyword:* Nerve morphometry

## 1. Introduction

Histopathological examination of peripheral nerves is often complemented by morphometric analysis in both clinical and research settings, for instance in the examination of regenerative nerve phenomena (Mezin et al., 1994). This can be achieved manually or using computer-based image analysis systems which are capable of automating the process to a varying degree. Although the terminology used for different methods of nerve morphometry varies, most authors agree that the measurement of individual axons or nerve fibres, for instance on electron micrographs or light photomicrographs, using a scale or ruled grid is a manual method (Mathews, 1968; Sharma and Thomas, 1974) and the requirement for no user input at all constitutes a fully automated method (Ellis et al., 1980). The use of a digitising tablet or mouse connected to a computer to record measurements obtained from tracing around a nerve image, whether on ultrastructural photographs (Friede and Beuche, 1985), digital images or images issued from a camera lucida projection (Ewart et al., 1989), is variably termed a manual (Mezin et al., 1994; Romero et al., 2000) or a semi-automated (Koller et al., 1997; Nehrer-Tairych et al., 2000) method, whereas the use of an automated technique which permits user interaction is variably termed semi-automated or semi-automated interactive (Mezin et al., 1994). In this discussion, the terms will be used as follows: 'manual' and 'fully automated' morphometry as used previously (Ellis et al., 1980; Mathews, 1968; Sharma and Thomas, 1974); semi-automated morphometry to refer to the use of a digitising tablet or similar to trace around nerve images; and interactive automated morphometry to refer to automated morphometry which permits user manipulation of data analysis.

Manual and semi-automated nerve morphometry are extremely tedious, labour intensive and time-consuming methods (Mezin et al., 1994), and operator fatigue and subjective decision-making are considered significant potential sources of error (Auer, 1994). To overcome this there have been efforts to devise representative sampling schemes to reduce the amount of data analysis required (Mathieu et al., 1981; Mayhew and Sharma, 1984a,b; Müller et al., 1981). However, the bimodal size distribution and extreme heterogeneity of local densities of myelinated fibres make the accuracy of results obtained using sampling dubious (Torch et al., 1989a).

An alternative is the use of fully automated morphometry, combining computer-based image analysis systems with

* Corresponding author. Tel.: +44 7939 868748; fax: +44 207 7937669.
*E-mail address:* fulvio@doctors.org.uk (F. Urso-Baiarda).

0165-0270/$ – see front matter © 2006 Elsevier B.V. All rights reserved.
doi:10.1016/j.jneumeth.2006.02.014

self-activating microscope stage displacement. The need for sampling is obviated by the rapidity of results obtained (Vita et al., 1992) with no requirement for human interaction. However, fully automated morphometry is associated with other problems, including the conversion of uncorrected errors in image interpretation to spurious data (Zimmerman et al., 1980), estimated at 8.3% (Usson et al., 1991). Interactive automated morphometry appears to have greater accuracy (Mezin et al., 1994) whilst retaining a reasonable output speed (Ellis et al., 1980; Mezin et al., 1994).

However, both fully and interactive-automated morphometry require specialised equipment to set up and are expensive techniques. They can also be difficult to implement because their methodological description in the literature is often in abstract terms (for instance, a mathematical description of the particle separation algorithms employed), using custom-made software which is not widely available (Ellis et al., 1980; Romero et al., 2000). There is therefore at present no method of nerve histomorphometry that fulfils all criteria of being readily available without additional specialised equipment, rapid enough to obviate sampling and accurate enough to produce meaningful data. In view of this, a novel method of nerve morphometry was developed aiming to fulfil the following principles:

(1) A fully automated component for rapid evaluation of most axons,
(2) A semi-automated component for slower evaluation of remaining axons and error correction,
(3) A software-based approach avoiding the need for specialised hardware, and
(4) The use of non-proprietary publicly available software for more widespread applicability of the method.

In order to assess the vailidity of this approach, the combined fully and semi-automated method was compared with a standard semi-automated method for nerve morphometry.

## 2. Materials and methods

### 2.1. Animal and tissue preparation

All operations were carried out in accordance with local ethical requirements for work involving animals and conformed to UK Home Office regulations. Two biopsies of each of the motor nerve to rectus femoris, marginal mandibular branch of the facial nerve and ventral ramus of buccal branch of the facial nerve were obtained from female New Zealand White Rabbits (2500–3500 g) to be used for control data in an unrelated experiment. Anaesthesia was induced with 0.7 ml intramuscular Hypnorm (Janssen, Oxford; fentanyl citrate 0.15 mg/ml; fluanisone 10 mg/ml) followed by 0.4 ml intravenous diazepam, and maintenance anaesthesia was achieved using intravenous fentanyl and fluanisone ('Hypnorm') as required. The nerves were dissected and a short sample excised distally.

Nerve biopsy specimens were processed immediately for histological and quantitative morphometric analysis. To maintain their length the nerve biopsies were stretched onto labelled white card and fixed overnight in a solution of PIPES buffered 2.5% glutaraldehyde solution (Baur and Stacey, 1977). The sample was washed in PIPES buffered 2% sucrose solution for 30 min and osmicated overnight in a 50:50 mixture of PIPES buffered 2% $OsO_4$ + 3% $K_3Fe(CN)_6 \cdot 3H_2O$ and PIPES buffered 6% $NaIO_3$ + 4% sucrose. It was then serially dehydrated in alcohol and impregnated with epoxy resin overnight (Langford and Coggeshall, 1980). After this, the labelled samples were embedded in fresh epoxy resin contained in a rubber mould for a further 24 h in an oven at 66 °C with a vacuum pressure of 15 psi. The resin blocks could then be removed from the moulds ready for sectioning.

Transverse 0.5 μm thickness sections were cut with a glass knife using an ultramicrotome (Reichert-Jung, Germany), collected in a knife-mounted 10% acetone bath and transferred to a clean glass slide on a drop of 10% acetone. They were then stretched using a chloroform-soaked wooden stick, dried gently over a methanol lantern, and stained and counter-stained with thionin and acridine orange. Once dry, a cover slip was mounted over the sections using epoxy resin and the sections examined under light microscopy.

### 2.2. Image acquisition

Overlapping colour digital photographs of each section were taken at 40× magnification using a microscope (Zeiss Axiophot) with a mounted digital camera (Leica), stored in lossless (.bmp) format and imported into a personal computer using Adobe Photoshop CS (Adobe Systems Inc., USA). The final image was automatically reconstituted from its component overlapping images using the 'Photomerge' command (File > Automate > Photomerge).

### 2.3. Image processing

#### 2.3.1. Standard semi-automated method

The semi-automated method of nerve morphometry was similar to that used elsewhere (Koller et al., 1997; Nehrer-Tairych et al., 2000). The image was enlarged by 500% and printed on 42-in. roll paper using a Hewlett Packard Design Jet 500 PS large format printer. Axon counting and area measurement were performed by systematically tracing each axonal outline using a digitising tablet (GTCO Calcomp Inc., Scottsdale, AZ) coupled to a personal computer (Fig. 1). Data was automatically imported into a spreadsheet package for further analysis.

#### 2.3.2. Combined automated and semi-automated method

Several commercially available (e.g. Image-Pro Plus, Media Cybernetics UK) and public domain (NIH Image, ImageJ) image analysis software packages permit rapid morphometric analysis of 'particles' within a digital image imported from a wide range of sources. ImageJ (Rasband, 1997–2005) was selected for its ready availability, extensive use in previous medical and scientific research (Bailey et al., 2002; Brown et al., 2005; Cho and Daniel, 2005; Gering and Atkinson, 2004; Girish and Vijayalakshmi, 2004; Lau et al., 2005; Williams et al., 2005),

Fig. 1. Nerve morphometry using a standard semi-automated digitizer pen method.

accessible user interface and versatility for future extended applications through the use of plug-ins.

Histomorphometry of the original nerve section image using ImageJ alone and axonal selection based on colour threshold adjustment was not sufficiently sensitive and specific, with threshold adjustments improving one at the expense of the other (Fig. 2a and b). Prior electronic subtraction of the background qualitatively improved specificity but increased image noise unacceptably (Fig. 2c). It was therefore necessary to prepare the image first using a different software package, Adobe Photoshop CS. After initial calibration, image analysis took place over four stages: image preparation; automated analysis; semi-automated analysis and data output.

*2.3.2.1. Calibration.* This step was performed once, as follows: a graticule image (0.01 mm, Wild, Switzerland) was captured under light microscopy using the same magnification and method as described earlier. This image was opened using ImageJ and the 'Straight line selections' tool was used to join two points on the graticule image of known physical dimensions. The Set Scale command (Analyze > Set Scale) was then selected. The 'Known Distance' and 'Unit of Length' boxes were completed based on dimensions read from the graticule, both the 'Pixel Aspect Ratio' (set at 1.00) and 'Distance in Pixels' (set according to the length measured by the 'Straight line selections tool') were left unchanged, and the 'Global' box was checked. The pixel size corresponded to 0.166 μm.

*2.3.2.2. Image preparation (Adobe Photoshop).* Image preparation using Adobe Photoshop is shown in Fig. 3. The 'Trace Contour' command (Filter > Stylize > Trace Contour) was used to provide an outline representation of the original image. The 'Level' setting was adjusted by trial and error to produce a darkest outline corresponding to the internal myelin edge (in this case to measure axons rather than nerve fibres). It was useful to select a value which also produced confluent nerve fibre (external myelin) outlines to speed up later processing, as described below. An optimal value was usually between 110 and 160. Non-axonal

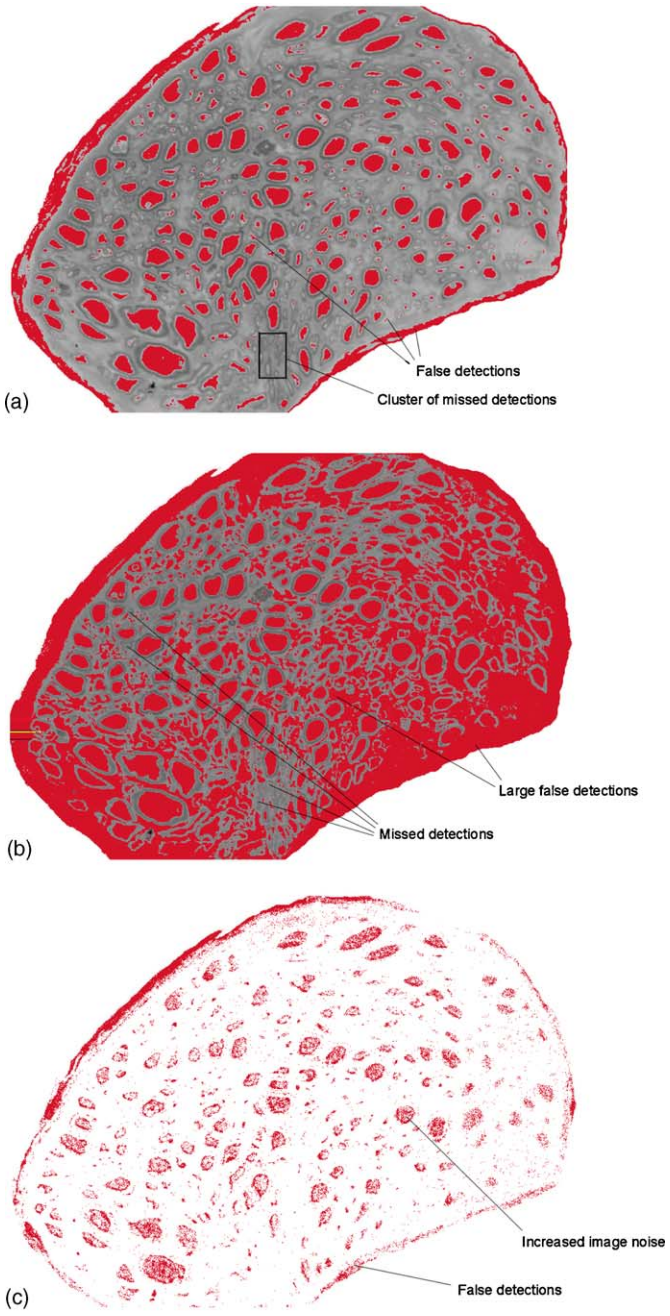


Fig. 2. Particle detection within a typical nerve biopsy image using ImageJ and varying the detection thresholds. The background image is shown in grayscale and software-detected particles are shown in red. Threshold adjustment produced either (a) more missed detections than false detections, or (b) more false detections than missed detections. In neither case was either type of error eliminated. Prior electronic background subtraction (c) incompletely reduced artefact selection and increased image noise. (For interpretation of the references to colour in this figure legend, the reader is referred to the web version of the article.)

outlines, rendered in yellow and turquoise, were automatically replaced with white using the 'Colour Replacement' command (Image > Adjustments > Replace Colour). The image was then converted to grayscale (Image > Mode > Grayscale) and saved.

*2.3.2.3. Automated particle detection (ImageJ).* The saved image (see Fig. 4) was opened in ImageJ and converted to a

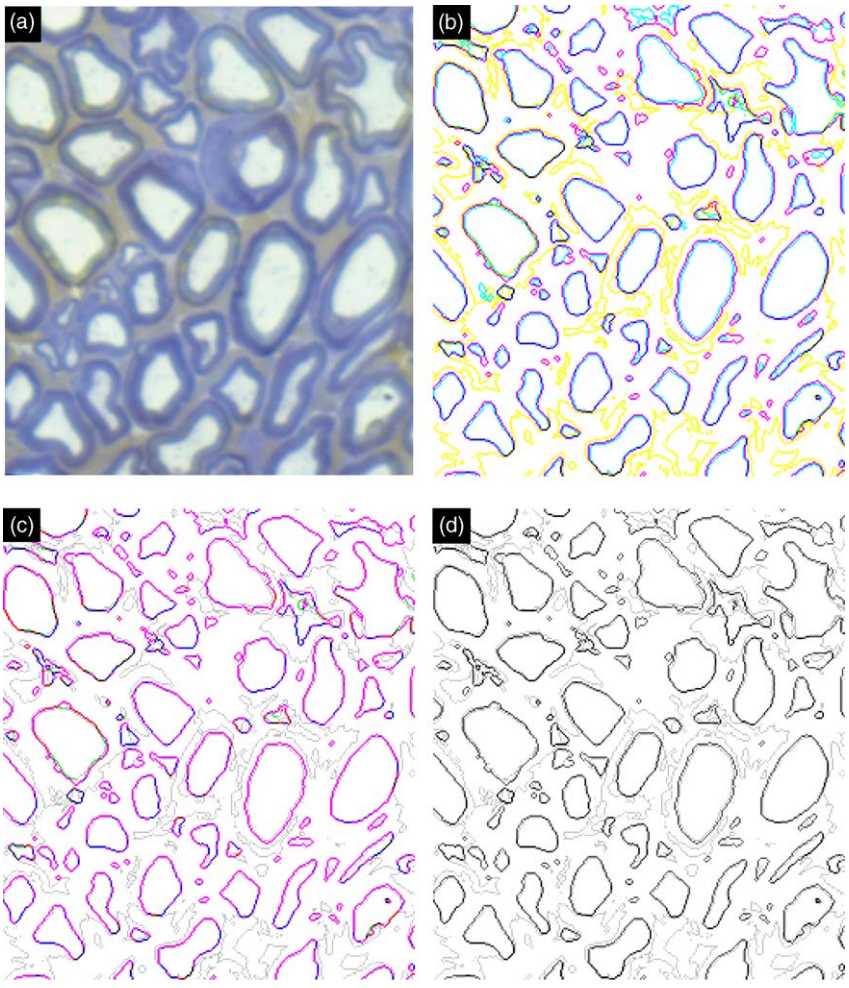


Fig. 3. Image preparation. (a) The original image has (b) a 'Trace Contour' command applied followed by (c) subtraction of non-axonal outlines rendered in yellow and turquoise. (d) The image is finally saved in grayscale. (For interpretation of the references to colour in this figure legend, the reader is referred to the web version of the article.)

binary (black and white) outline image by threshold adjustment (Image > Adjust > Threshold), in which an intensity threshold was set above and below which all grays were converted to black and white, respectively. This produced an image of individual axonal outlines, as well as outlines of interstitial artefact and of the entire fascicle(s). Before particle analysis could be performed it was necessary to use the eraser tool to make the fascicular outline discontinuous by at least one pixel, to prevent the analysis from recognising the fascicle as a single large particle and ignoring axons within it. Similarly, any external myelin outlines had to be interrupted by at least one pixel to allow the software to recognise the axonal outlines within them. If the Trace Contour setting selected previously rendered the external myelin outlines confluent then only a single interruption anywhere along the confluent circumference was required.

Automated image analysis was then performed (Analyze > Analyze Particles; Set 'Show' to 'Masks' and uncheck all boxes), producing an image in which axons were represented as solid black areas. Error from both missed detections and interstitial and external artefact were also apparent. These took the form of solid black areas or black outlines, depending on whether its outline had been broken using the eraser tool earlier. Linear artefact could be rapidly removed using the 'Smooth' command to blur it (Process > Smooth) followed by repeating the threshold adjustment (Image > Adjust > Threshold) to filter out blurred lines while retaining solid black areas. This image was saved.

*2.3.2.4. Semi-automated particle detection (Adobe Photoshop).* The image obtained thus far still contained solid areas of interstitial and other artefact, as well as a few axons that had not been detected. Such errors were corrected by semi-automated analysis: the most recent binary image was opened as a semi-opaque layer over the original nerve image (Fig. 5a) in Photoshop CS, permitting visual assessment of the accuracy of automated analysis. The image was systematically inspected frame by frame and any errors manually corrected onto the binary layer using standard drawing tools (Fig. 5b). A white 'Fill' tool was particularly useful for removing large areas of artefact, especially confluent interstitial artefact, whilst a black or white 'Pencil' tool was useful for more minor corrections. When finished, the binary layer opacity was returned to 100% and the corrected binary image was saved (Fig. 5c).

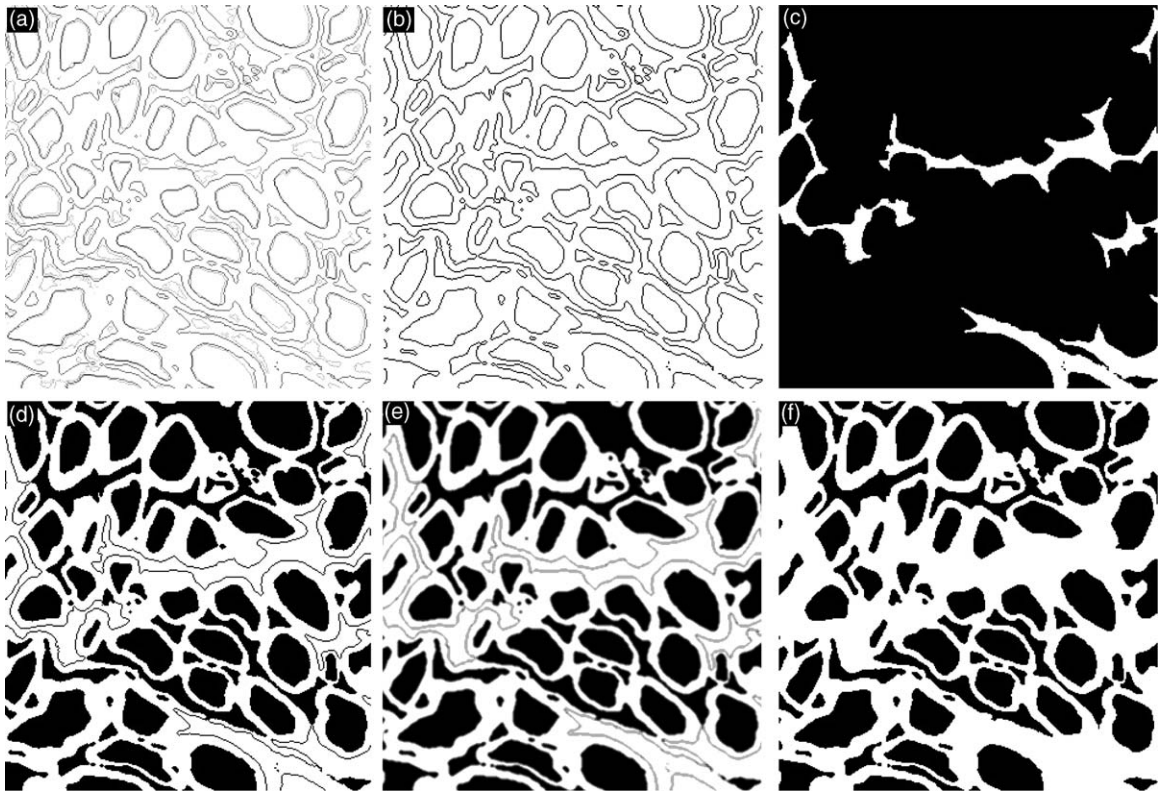


Fig. 4. Automated particle detection using ImageJ. (a) The original grayscale image is opened and (b) converted to a binary image by thresholding. (c) In order to prevent recognition of a single large particle, (d) the external fascicular and confluent myelin outlines must be interrupted. Linear artefact is then removed by (e) performing the smooth command to blur it, followed by (f) repeating the threshold command.

*2.3.2.5. Data output (ImageJ).* This image was finally reopened in ImageJ for final particle analysis (Analyze > Analyze Particles). Setting 'Show' to 'Masks' provided an image of axons that had been detected, and to 'Outline' provided a labeled image, both of which were occasionally useful for quality control purposes. The 'Display Results' box was checked to provide individual particle measurements, the 'Size Distribution' box for a particle size histogram and the 'Summarize' box

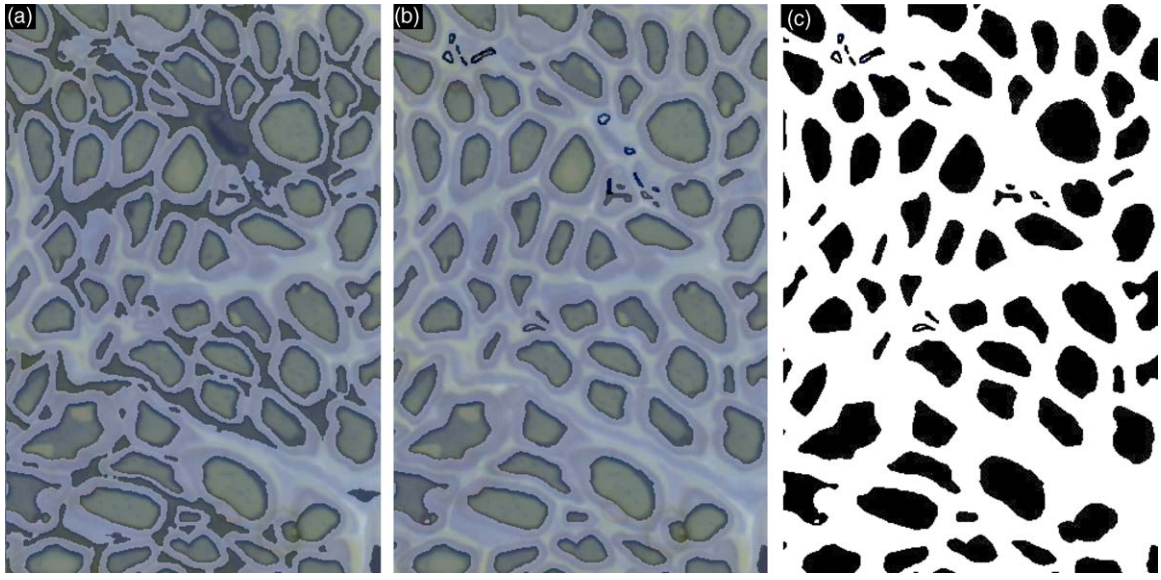


Fig. 5. Semi-automated particle analysis. (a) Errors of missed detection and false detection, usually of interstitial artefact, are apparent by overlaying the last saved image as a semi-opaque layer over the original image. (b) Errors are then systematically removed frame by frame, (c) resulting in a corrected binary image representing axons.

Table 1
Axon number, mean axonal area and analysis time using traditional semi-automated and combined automated & semi-automated methods

| Nerve | Axon no. | | Mean axon area ($\mu m^2$) (S.D.) | | Analysis time (min) | |
|---|---|---|---|---|---|---|
| | Semi-automated method | Combined method (% semi-automated) | Semi-automated method | Combined method (% semi-automated) | Semi-automated method | Combined method (% semi-automated) |
| Rectus | | | | | | |
| 1 | 790 | 780 (98.7%) | 56.1 (54.8) | 55.3 (51.2) | 140 | 52 (37.1%) |
| 2 | 719 | 763 (106.1%) | 32.2 (30.3) | 32.4 (32.3) | 121 | 43 (35.5%) |
| MM | | | | | | |
| 3 | 315 | 334 (106.0%) | 19.3 (12.8) | 17.5 (12.4) | 55 | 23 (41.8%) |
| 4 | 614 | 615 (100.2%) | 13.9 (9.3) | 17.2 (11.4) | 88 | 39 (44.3%) |
| VRB | | | | | | |
| 5 | 4190 | 3991 (95.3%) | 20.4 (12.8) | 20.2 (12.9) | 1140 | 395 (34.6%) |
| 6 | 5301 | 5513 (104.0%) | 16.3 (12.0) | 16.6 (12.1) | 1462 | 480 (32.8%) |

Rectus: motor nerve to rectus femoris; MM: marginal mandibular branch of facial nerve; VRB: ventral ramus of buccal branch of facial nerve.

for descriptive statistics of the data. The data obtained could then be exported directly into other statistics or spreadsheet software for further analysis.

### 2.4. Statistical methods

Results obtained using each method were compared for axon count, axonal area and analysis time per nerve section. Each method was compared using the independent samples *t*-test for mean axonal area, Pearson correlation for axon counts and Wilcoxon signed ranks test for axon counts and time taken to perform image analysis.

## 3. Results

The results are summarised in Table 1.

### 3.1. Axon counts

Axon counts using the combined fully and semi-automated method ranged from 98.7% to 106.1% of the axon count using the semi-automated method alone, with a Pearson correlation of 0.998 (Fig. 6). There was no significant difference between axon counts performed by either method ($p = 0.600$).

### 3.2. Axonal area

Mean axonal areas for each nerve using both the combined and semi-automated methods are summarised in Fig. 7. There was no significant difference in mean axonal area obtained using either method for any nerve ($p = 0.211$–$0.928$). Moreover, each nerve displayed a characteristic nerve size frequency distribution that exhibited good correlation between methods (Fig. 8, Pearson correlations of 0.860, 0.958, 0.884, 0.955, 0.997 and 0.995, for nerves 1–6 respectively, $p < 0.001$ each).

### 3.3. Analysis time

The semi-automated method took between two and three times longer to perform than the combined method, which was statistically significant ($p = 0.028$, Table 1). There appeared to be an inverse relationship between axon number and ratio of combined:semi-automated analysis time, suggesting greatest benefit in terms of analysis time from the combined

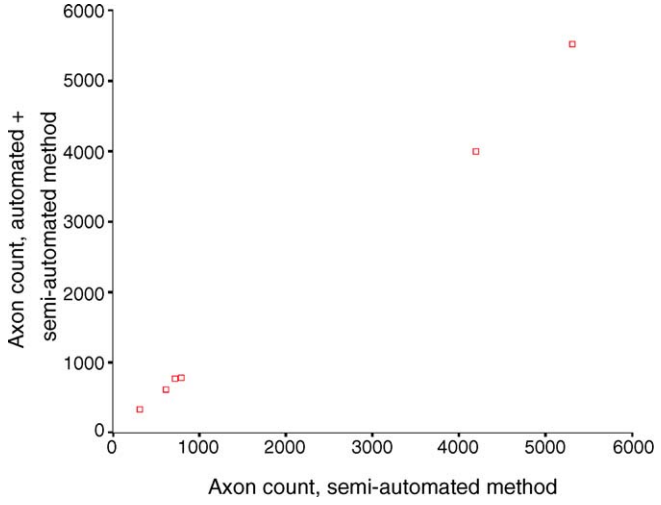


Fig. 6. Correlation between axon counts obtained using combined or semi-automated morphometry (Pearson correlation = 0.998, $p < 0.01$).

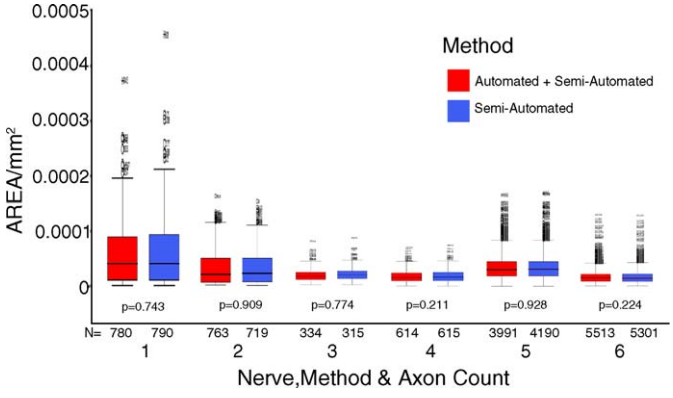


Fig. 7. Axonal area assessed using the combined or semi-automated methods. Mean axonal area was statistically similar using either method for all nerves ($p = 0.211$–$0.928$).

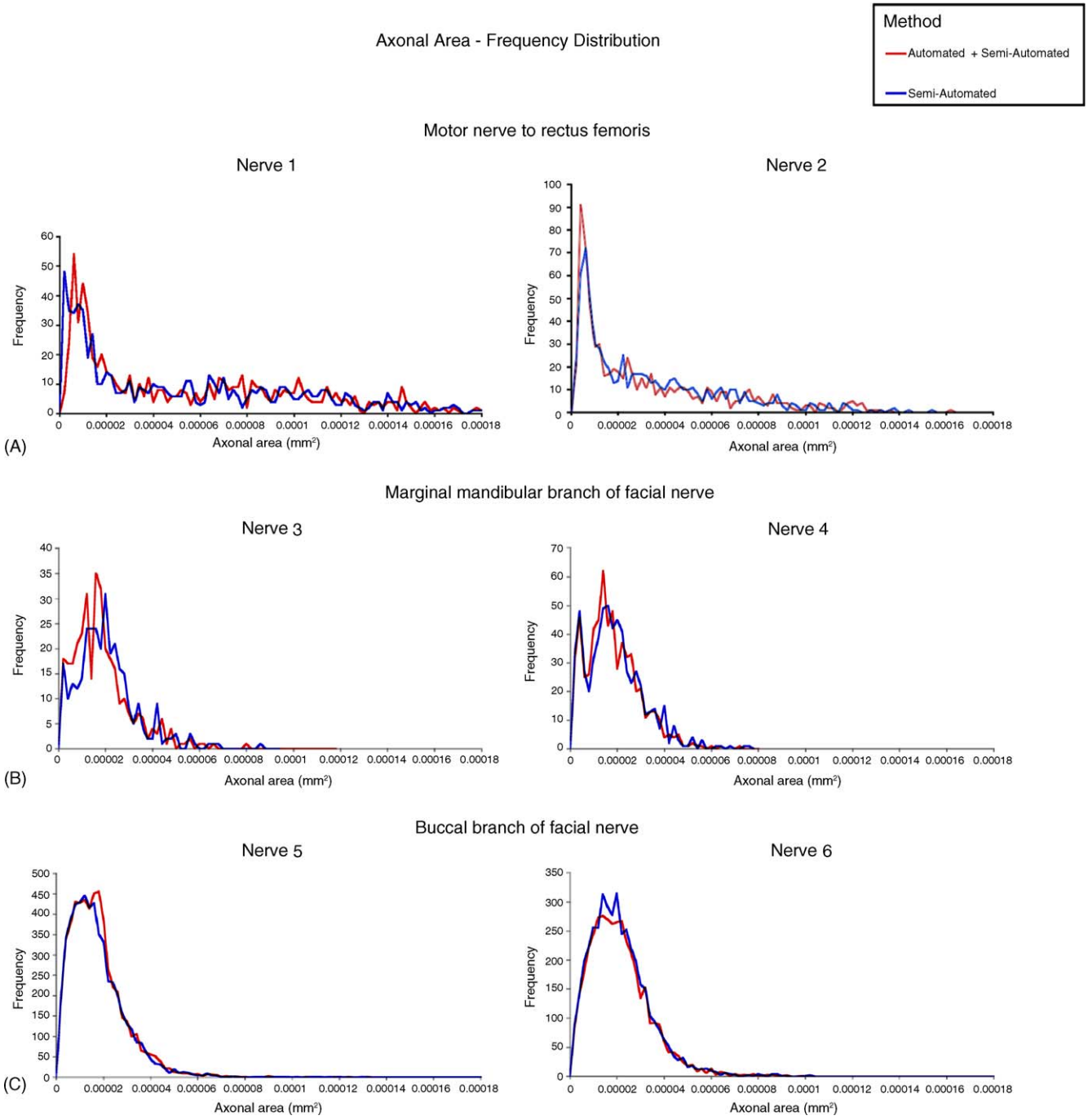


Fig. 8. Frequency distribution of axonal area using the combined or semi-automated methods (Pearson correlation = 0.860–0.997, $p < 0.01$).

method for nerves containing most axons (Pearson correlation −0.734), although this relationship was not statistically significant ($p = 0.097$).

## 4. Discussion

Traditional methods of quantifying histopathological examination of peripheral nerves have several disadvantages. Manual or semi-automated morphometry are tedious, labour intensive and time-consuming processes, likely to attract error through operator fatigue and subjective decision-making (Auer, 1994). With semi-automated analysis of a medium-sized peripheral nerve taking a whole day's work (Mezin et al., 1994) and manual analysis taking even longer, their use is limited by the finite time available for a research project. Whilst isolated studies report good mean peripheral nerve fibre diameter estimation from small sample sizes (e.g. 185/2900 fibres) (Mayhew and Sharma, 1984a), others indicate that at least 50% sampling is necessary to achieve accurate area and perimeter estimations (Torch et al., 1989a). Torch et al. (1989a) considers sampling methods for nerve morphometry flawed by the bimodal size distribution and extreme heterogeneity of local densities of myelinated fibres.

The main advantages of fully automated morphometry are, through avoidance of human input, loss of subjective decision-making and an increase in processing speed, which may in turn obviate the need for sampling. For instance, average processing speeds of approximately 1.5–10 s per analysed nerve fibre are quoted for fully automated methods (Ellis et al., 1980; Romero et al., 2000; Selva et al., 1981) compared with 20–40 s per analysed nerve fibre for semi-automated methods (Mezin et al., 1994; Romero et al., 2000). Unfortunately, increased processing speed occurs at the expense of accuracy with fully automated nerve morphometry. Algorithms used to discriminate nerve fibre from background or artefactual features may not work from time to time, and without human quality-control uncorrected errors in image interpretation are converted to spurious data, estimated at around 8% (Usson et al., 1991).

A common error in automated nerve morphometry is the interpretation of close or overlapping 'particles' as single particles. This may explain why early work on automated image analysis concentrated on analysis of cytological specimens (Diacymakos et al., 1962; Prewitt and Mendelsohn, 1966) and greatest success to date has been in the analysis of blood smears, with fast execution rates and accuracy equalling human performance (Preston and Bartels, 1988). Another source of error in automated nerve morphometry is the false positive, caused by inappropriate recognition of artefact such as excessive stain, or of background features such as connective tissue, blood vessels, blood cells or degenerate axons. A third type of error is missed detection of true axons, arising because algorithms typically reject rather than correct maldetected axons such as those with a break along their boundary (Ellis et al., 1980). In this regard, the accuracy of automated morphometry is sensitive to the quality of section and, in particular, how well it is stained. Several authors have remarked on the underestimation of numbers of small or regenerating axons by automated morphometry (Ellis et al., 1980; Usson et al., 1991; Vita et al., 1992) since their thin, poorly staining myelin provide insufficient contrast with the interstitial space for automatic detection.

Few studies have attempted to quantify the error encountered with the use of fully automated morphometry. This may be because the amount of work required to generate accurate control data considerably restricts the sample size that can be practically achieved. One study, however, compared their own fully automated morphometric technique with a standard semi-automated approach[1] for a single cat sciatic nerve biopsy (Romero et al., 2000). In that study, 3434 nerve fibres were detected manually compared with 3256 detected automatically (94.8% of semi-automated count), from which 33 (1.0%) were considered as false detections and 211 (6.1%) as missed detections. It is not possible to know whether other automated methods, or indeed increased sample sizes using the previous method, would achieve that degree of accuracy.

Other evidence suggests that this may not be the case. Comparison of fibre numbers analysed using fully automated and interactive automated methods has revealed differences of 14.4% (Selva et al., 1981) and 16% (Savy et al., 1987), whilst a comparison of myelinated fibre number analysed using interactive automated and semi-automated morphometry[2] displayed a non-significant 0.8% difference and 0.6% inter-observer variability between two users performing five repeats (Mezin et al., 1994). Since the correlation between interactive automated and semi-automated methods is high (Mezin et al., 1994), moderate discrepancies between fully automated and interactive automated techniques in the studies by Selva et al. (1981) and by Savy et al. (1987) are more likely to reflect error inherent to full automation.

Improved accuracy of interactive automated morphometry compared with the fully automated approach does not appear to be at the detriment of sampling rate, with reported rates of 3.5–7 s per analysed nerve fibre (Mezin et al., 1994; Torch et al., 1989b), similar to those published for fully automated nerve morphometry. This may be due to the need for human intervention for only a small proportion of axons, allowing average analysis rates to approximate those of fully automated morphometry. However, other impediments to the use of fully automated morphometry apply equally to interactive-automated morphometry. Both require dedicated laboratory space, specialised equipment and therefore significant set-up costs. Automated or interactive automated processes can also be difficult to implement because their methodological description in the literature is often in conceptual or mathematical rather than practical terms, using custom-made software which is not widely available (Ellis et al., 1980; Romero et al., 2000). Thus reproduction of the described methodology would require the de novo production of software based on the principles described.

There is therefore at present no method of nerve histomorphometry that is readily available without additional specialised equipment, rapid enough to obviate sampling and accurate enough to produce reliable data. In view of this, a novel method of software-based nerve morphometry was developed combining fully automated and semi-automated techniques. This system is conceptually similar to that described by Zimmerman et al. (1980) in which over 85% of axons were detected automatically, followed by semi-automatic elimination of errors of inclusion, exclusion and overlap. However, the latter had significant hardware requirements. Our results indicate that the combined fully and semi-automated software-based method of nerve morphometry correlates highly with data obtained using a traditional semi-automated technique, whilst taking significantly less time to perform.

Such an approach is attractive for several reasons. It is inexpensive to set up, requiring in addition to standard laboratory equipment only a computer running two readily available software packages, with negligible running costs. This method does not require dedicated laboratory space, and is indeed portable, allowing work to take place opportunistically when

[1] This paper used different morphometry terminology, describing semi-automated morphometry using a digital image and mouse as 'manual'.

[2] Similarly, this paper described interactive automated morphometry as 'semi-automated', and semi-automated morphometry using a digitizing tablet as 'manual'.

time becomes available. The method is also rapid enough to avoid data sampling and provides a record of the exact outlines that have been measured for comparison with the original image, permitting subsequent critical evaluation of the quality of data obtained. If errors are noted at a later date it is possible to correct these and repeat the analysis in only a few seconds. We envisage the use of this method may be extended to the morphometry of other tissues, such as smooth or skeletal muscle. We are currently developing a modification of the method of nerve morphometry presented here for morphometric analysis of skeletal muscle.

Whilst the method described uses two separate software packages, ImageJ has the capacity for extended functionality through the use of plug-ins. Developers may in the future wish to incorporate features currently requiring the use of separate software, in this case Adobe Photoshop CS, within ImageJ in order to provide an integrated solution to morphometry in a single software package that can be run on any Java-enabled platform, including Windows, Mac OS and Linux.

## References


Auer RN. Automated nerve fibre size and myelin sheath measurement using microcomputer-based digital image analysis: theory, method and results. J Neurosci Methods 1994;51:229–38.

Bailey SR, Polan JL, Morse B, Wetherold S, Villanueva-Vedia RE, Waggoner D, Phelix C, Barera-Roderiquiz E, Goswami N, Munoz O, Agrawal CM. Angiogenic bFGF expression from gas-plasma treated scaffolds. Cardiovasc Radiat Med 2002;3:183–9.

Baur PS, Stacey TR. The use of PIPES buffer in the fixation of mammalian and marine tissues for electron microscopy. J Microsc 1977;109:315–27.

Brown KM, Donohue DE, D'Alessandro G, Ascoli GA. A cross-platform freeware tool for digital reconstruction of neuronal arborizations from image stacks. Neuroinformatics 2005;3:343–60.

Cho WJ, Daniel EE. Colocalization between caveolin isoforms in the intestinal smooth muscle and interstitial cells of Cajal of the Cav1(+/+) and Cav1(−/−) mouse. Histochem Cell Biol 2005:1–8.

Diacymakos EG, Day E, Kopac MJ. Exfoliated cell studies and the cytoanalyser. Ann NY Acad Sci 1962;97:329.

Ellis TJ, Rosen D, Cavanagh JB. Automated measurement of peripheral nerve fibres in transverse section. J Biomed Eng 1980;2:272–80.

Ewart DP, Kuzon WM, Fish JS, McKee NH. Nerve fibre morphometry: a comparison of techniques. J Neurosci Methods 1989;29:143–50.

Friede RL, Beuche W. Combined scatter diagrams of sheath thickness and nerve calibre in human sural nerves: changes with age and neuropathy. J Neurol Neurosurg Psychiat 1985;48:749–56.

Gering E, Atkinson CT. A rapid method for counting nucleated erythrocytes on stained blood smears by digital image analysis. J Parasitol 2004;90:879–81.

Girish V, Vijayalakshmi A. Affordable image analysis using NIH Image/Image. J Indian J Cancer 2004;41:47.

Koller R, Rab M, Todoroff BP, Neumayer C, Haslik W, Stohr HG, Frey M. The influence of the graft length on the functional and morphological result after nerve grafting: an experimental study in rabbits. Br J Plast Surg 1997;50:609–14.

Langford LA, Coggeshall RE. The use of potassium ferricyanide in neural fixation. Anat Rec 1980;197:297–303.

Lau D, Seibert A, Gandara D, Laptalo L, Geraghty E, Coulon C. Computer-assisted image analysis of bronchioloalveolar carcinoma. Clin Lung Cancer 2005;6:281–6.

Mathews MA. An electron microscopic study of the relationship between axon diameter and the initiation of myelin production in the peripheral nervous system. Anat Rec 1968;161:337–52.

Mathieu O, Cruz-Orive LM, Hoppeler H, Weibel ER. Measuring error and sampling variation in stereology: comparison of the efficiency of various methods for planar image analysis. J Microsc 1981;121:75–88.

Mayhew TM, Sharma AK. Sampling schemes for estimating nerve fibre size. I. Methods for nerve trunks of mixed fascicularity. J Anat 1984a;139:59–66.

Mayhew TM, Sharma AK. Sampling schemes for estimating nerve fibre size. II. Methods for unifascicular nerve trunks. J Anat 1984b;139:59–66.

Mezin P, Tenaud C, Bosson JL, Stoebner P. Morphometric analysis of the peripheral nerve: advantages of the semi-automated interactive method. J Neurosci Methods 1994;51:163–9.

Müller AE, Cruz-Orive LM, Gehr P, Weibel ER. Comparison of two subsampling methods for electron microscopy morphometry. J Microsc 1981;1231:35–49.

Nehrer-Tairych GV, Rab M, Kamolz L, Deutinger M, Stohr HG, Frey M. The influence of the donor nerve on the function and morphology of a mimic muscle after cross innervation: an experimental study in rabbits. Br J Plast Surg 2000;53:669–75.

Preston KJ, Bartels PH. Progress in medical imaging. New York: Springer-Verlag; 1988.

Prewitt JMS, Mendelsohn ML. The analysis of cell images. Ann NY Acad Sci 1966;128:1035.

Rasband WS, 1997–2005. ImageJ, USNIo Health, Bethesda, Maryland, USA.

Romero E, Cuisenaire O, Denef JF, Delbeke J, Macq B, Veraart C. Automatic morphometry of nerve histological sections. J Neurosci Methods 2000;97:111–22.

Savy C, Margules S, Solari A, Saint-Jean P, Farkas-Bargeton E. An image analysis morphometric method for the study of myelinated nerve fibers from mouse trigeminal root. Anal Quant Cytol Histol 1987;10: 307–16.

Selva J, Schoëvaërt-Brossault D, Said G. Automated morphometric analysis of cross-sections of normal and pathological nerve biopsy specimens. Biol Cell 1981;42:57–64.

Sharma AK, Thomas PK. Peripheral nerve structure and function in experimental diabetes. J Neurol Sci 1974;23:1–15.

Torch S, Stoebner P, Usson Y, Drouet D'Aubigny G, Saxod R. There is no simple adequate sampling scheme for estimating the myelinated fibre size distribution in human peripheral nerve: a statistical ultrastructural study. J Neurosci Methods 1989a;27:149–64.

Torch S, Usson Y, Saxod R. Automated morphometric study of human peripheral nerves by image analysis. Pathol Res Pract 1989b;18:567–71.

Usson Y, Torch S, Saxod R. Morphometry for human nerve biopsies by means of automated cytometry: assessment with reference to ultrastructural analysis. Anal Cell Pathol 1991;3:91–102.

Vita G, Santoro M, Trombetta G, Leonardi L, Messina C. A computer-assisted automatic method for myelinated nerve fiber morphometry. Acta Neurol Scand 1992;85:18–22.

Williams SM, Bryan-Lluka LJ, Pow DV. Quantitative analysis of immunolabeling for serotonin and for glutamate transporters after administration of imipramine and citalopram. Brain Res 2005;1042: 224–32.

Zimmerman IR, Karnes JL, O'Brien PC, Dyck PJ. Imaging system for nerve and fiber tract morphometry: components, approaches, performance and results. J Neuropathol Exp Neurol 1980;39:409–19.